

# Bisubstrate Analogue Inhibitors of 6-Hydroxymethyl-7,8-dihydropterin Pyrophosphokinase: Synthesis and Biochemical and Crystallographic Studies<sup>†</sup>

Genbin Shi,<sup>§,¶</sup> Jaroslaw Blaszczyk,<sup>||,¶</sup> Xinhua Ji,<sup>\*,||</sup> and Honggao Yan<sup>\*,§</sup>

Department of Biochemistry and Molecular Biology, Michigan State University, East Lansing, Michigan 48824, and Macromolecular Crystallography Laboratory, National Cancer Institute, Frederick, Maryland 21702

Received October 20, 2000

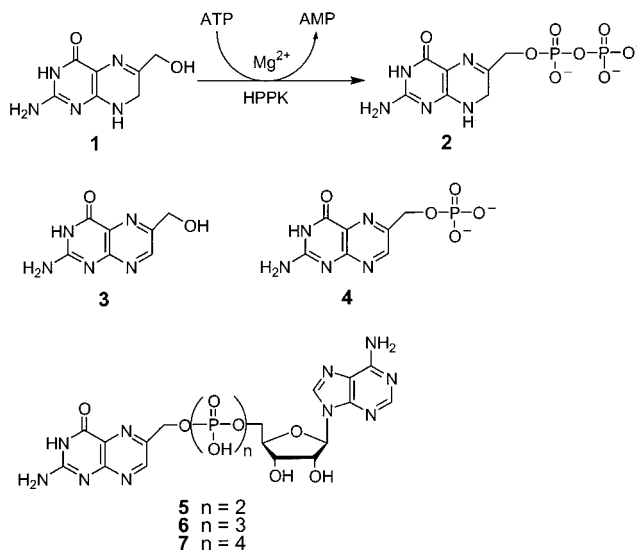
6-Hydroxymethyl-7,8-dihydropterin pyrophosphokinase (HPPK) catalyzes the transfer of pyrophosphate from ATP to 6-hydroxymethyl-7,8-dihydropterin (HP), leading to the biosynthesis of folate cofactors. Like other enzymes in the folate pathway, HPPK is an ideal target for the development of antimicrobial agents because the enzyme is essential for microorganisms but is absent from human and animals. Three bisubstrate analogues have been synthesized for HPPK and characterized by biochemical and X-ray crystallographic analyses. All three bisubstrate analogues consist of a pterin, an adenosine moiety, and a link composed of 2–4 phosphoryl groups. *P*<sup>1</sup>-(6-Hydroxymethylpterin)-*P*<sup>2</sup>-(5'-adenosyl)diphosphate (HP<sub>2</sub>A, **5**) shows little affinity and inhibitory activity for *E. coli* HPPK. *P*<sup>1</sup>-(6-Hydroxymethylpterin)-*P*<sup>3</sup>-(5'-adenosyl)triphosphate (HP<sub>3</sub>A, **6**) shows moderate affinity and inhibitory activity with  $K_d = 4.25 \mu\text{M}$  in the presence of  $\text{Mg}^{2+}$  and  $\text{IC}_{50} = 1.27 \mu\text{M}$ . *P*<sup>1</sup>-(6-Hydroxymethylpterin)-*P*<sup>4</sup>-(5'-adenosyl)tetrakisphosphate (HP<sub>4</sub>A, **7**) shows the highest affinity and inhibitory activity with  $K_d = 0.47 \mu\text{M}$  in the presence of  $\text{Mg}^{2+}$  and  $\text{IC}_{50} = 0.44 \mu\text{M}$ . The affinity of  $\text{MgHP}_4\text{A}$  for HPPK is  $\sim 116$  and  $76$  times higher than that of  $\text{MgADP}$  and 6-hydroxymethylpterin, respectively. The crystal structure of HPPK in complex with **7** (HPPK· $\text{MgHP}_4\text{A}$ ) has been determined at  $1.85 \text{ \AA}$  resolution with a crystallographic *R* factor of 0.185. The crystal structure shows that **7** occupies both HP- and ATP-binding sites and induces significant conformational changes in HPPK. The biochemical and structural studies of the bisubstrate analogues indicate that the bisubstrate analogue approach can produce more potent inhibitors for HPPK and the minimum length of the link for a bisubstrate analogue is  $\sim 7 \text{ \AA}$ .

## Introduction

Rapidly increasing antibiotic resistance in recent years has rendered the current antibiotics ineffective for treating many microbial infections, resulting in a worldwide health care crisis.<sup>1–5</sup> According to a 1999 WHO report,<sup>6</sup> infectious diseases are the leading causes of death and the main causes of premature death in the world. The crisis is further aggravated by the fact that most new antibiotics are chemical modifications of the basic structures of existing antimicrobial agents against old targets and thus less effective against widespread antibiotic resistance. Therefore, new targets for developing novel antimicrobial agents are urgently needed for combating the antibiotic crisis.

6-Hydroxymethyl-7,8-dihydropterin pyrophosphokinase (HPPK) catalyzes the transfer of pyrophosphate from ATP to 6-hydroxymethyl-7,8-dihydropterin (HP) (Chart 1), the first reaction in the folate biosynthetic pathway.<sup>7</sup> Folate cofactors are essential for life.<sup>8</sup> Mammals have an active transport system for deriving folates from their diet. In contrast, most microorganisms must synthesize folates de novo because they lack the

**Chart 1.** Reaction Catalyzed by HPPK and Chemical Structures of the Bisubstrate Analogues and Key Precursors<sup>a</sup>



<sup>a</sup> **1**, 6-hydroxymethyl-7,8-dihydropterin; **2**, 6-hydroxymethyl-7,8-dihydropterin pyrophosphate; **3**, 6-hydroxymethylpterin; **4**, 6-hydroxymethylpterin monophosphate (HP<sub>2</sub>A); **5**, *P*<sup>1</sup>-(6-hydroxymethylpterin)-*P*<sup>2</sup>-(5'-adenosyl)diphosphate (HP<sub>3</sub>A); **6**, *P*<sup>1</sup>-(6-hydroxymethylpterin)-*P*<sup>3</sup>-(5'-adenosyl)triphosphate; **7**, *P*<sup>1</sup>-(6-hydroxymethylpterin)-*P*<sup>4</sup>-(5'-adenosyl)tetrakisphosphate (HP<sub>4</sub>A).

<sup>†</sup> The coordinates and structure factors have been deposited with the Protein Data Bank: accession code 1ex8.

\* To whom correspondence should be addressed. Tel: (517) 353-8786 (H.Y.); (301) 846-5035 (X.J.). Fax: (517) 353-9334 (H.Y.); (301) 846-6073 (X.J.). E-mail: yanhpilot.msu.edu (H.Y.); jix@ncifcrf.gov (X.J.).

<sup>§</sup> Michigan State University.

<sup>||</sup> National Cancer Institute.

<sup>¶</sup> These authors contributed equally to this work.

active transport system. Therefore, the folate biosynthetic pathway is an ideal target for developing anti-

microbial agents. Inhibitors of dihydropteroate synthase<sup>9</sup> and dihydrofolate reductase,<sup>10</sup> the second and fourth enzymes in the folate pathway, are currently used as antibiotics for treating many infectious diseases. HPPK represents a new target in a biosynthetic pathway that has been proven effective for the development of antimicrobial agents.

Because of its small size and high thermal stability,<sup>11,12</sup> HPPK is also an excellent model enzyme for studying the mechanisms of enzymatic pyrophosphoryl transfer. Although the mechanisms of many kinases that catalyze monophosphoryl transfer have been extensively characterized, little is known about the mechanisms of pyrophosphokinases.<sup>13</sup>

To seek an effective approach to make potent inhibitors for HPPK and probe the mechanism of the enzyme, we have synthesized three bisubstrate analogues (Chart 1). All three bisubstrate analogues consist of a pterin, an adenosine moiety, and a link composed of 2–4 phosphoryl groups. Biochemical analysis of the bisubstrate analogues has shown that *P*<sup>1</sup>-(6-hydroxymethylpterin)-*P*<sup>1</sup>-(5'-adenosyl)tetrphosphate (HP<sub>4</sub>A, **7**) is the most potent inhibitor of HPPK. The crystal structure of HPPK in complex with **7** (HPPK·MgHP<sub>4</sub>A) has been determined at 1.85 Å resolution with a crystallographic *R* factor of 0.185.

## Results

**Synthesis.** The bisubstrate analogues were synthesized by the method of Hoard and Ott.<sup>14</sup> Our initial attempt was to activate ATP with 1,1'-carbonyldiimidazole and then mix it in situ with 6-hydroxymethylpterin (**3**), but this was not successful. 6-Hydroxymethylpterin monophosphate (HPP, **4**) was then synthesized by the method of Ho et al.<sup>15</sup> The compound was activated with 1,1'-carbonyldiimidazole and treated in situ with AMP, ADP, or ATP. The yields for HPP (**4**), HP<sub>2</sub>A (**5**), HP<sub>3</sub>A (**6**), and HP<sub>4</sub>A (**7**) were ca. 65%, 31%, 35%, and 16%, respectively. The proton NMR spectrum of **4** showed two methylene protons as a doublet from splitting by phosphate. The phosphate chemical shift (2.84 ppm) of HPP was very similar to that (3.13 ppm) of AMP. The <sup>31</sup>P NMR spectra of **5–7** showed characteristic peaks at approximately –11 and –22 ppm corresponding to the terminal and middle phosphates, respectively. The <sup>31</sup>P chemical shifts were very similar to those reported for *P*<sup>1</sup>-(5'-adenosyl)-*P*<sup>*n*</sup>-(5'-thymidyl)-polyphosphate.<sup>16,17</sup>

**Biochemical Studies.** Representative titration curves for the inhibition and binding studies are shown in Figure 1a,b, respectively. The IC<sub>50</sub> and *K*<sub>d</sub> values obtained by nonlinear least-squares analysis of the data are summarized in Table 1. Among the three bisubstrate analogues, **7** was the most potent inhibitor of HPPK with IC<sub>50</sub> = 0.44 μM. The IC<sub>50</sub> of **6** was about 3 times of that of **7**. At a concentration of 100 μM, **5** showed little inhibition of HPPK activity. The *K*<sub>d</sub> values measured in the presence of Mg<sup>2+</sup> were very similar to the corresponding IC<sub>50</sub> values. In the absence of Mg<sup>2+</sup>, the *K*<sub>d</sub> values increased by about a factor of 4.

**Crystal Structure of HPPK·MgHP<sub>4</sub>A.** The 1.85 Å crystal structure of HPPK·MgHP<sub>4</sub>A (Figure 2a) contains 1 HPPK molecule, 1 HP<sub>4</sub>A molecule, 1 Mg<sup>2+</sup> ion, 1 Cl<sup>1-</sup> ion, and 167 water molecules. The HP<sub>4</sub>A molecule,

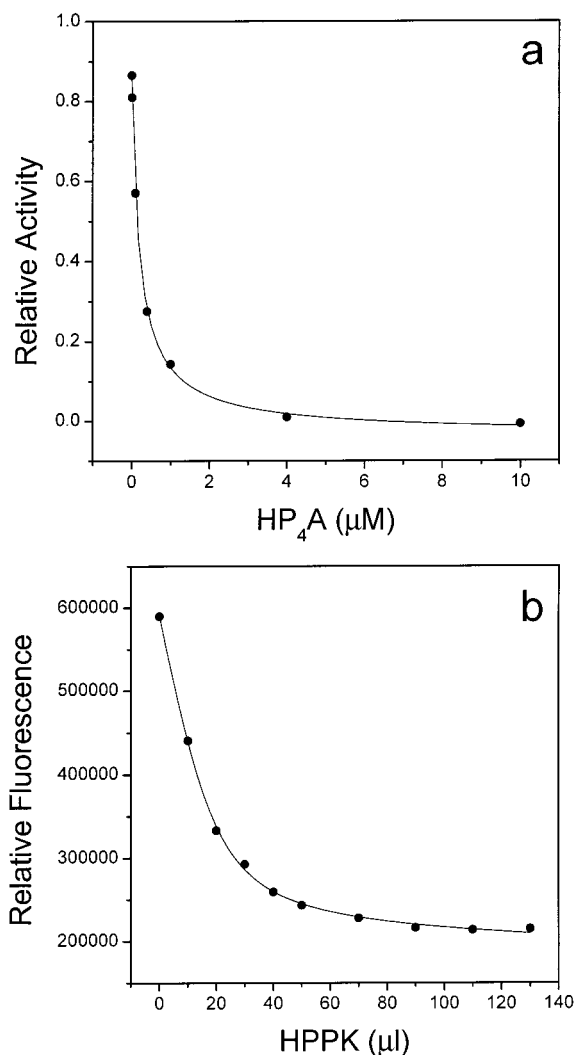


**Figure 1.** (a) Inhibition of HPPK by HP<sub>4</sub>A. The solid line was obtained by nonlinear least-squares fit of the experimental data. The details of the assay are described in the Experimental Section. (b) Fluometric titration of HP<sub>4</sub>A with HPPK. The concentration of the HPPK stock solution was 190 μM. The solid line was obtained by nonlinear least-squares fit of the data as described in the Experimental Section.

**Table 1.** Summary of the IC<sub>50</sub> and *K*<sub>d</sub> Values Obtained by Inhibition and Binding Studies

	HP <sub>2</sub> A	HP <sub>3</sub> A	HP <sub>4</sub> A
<i>K</i> <sub>d</sub> (μM) (without Mg <sup>2+</sup> )	nd	17.4 ± 1.5	1.93 ± 0.05
<i>K</i> <sub>d</sub> (μM) (with Mg <sup>2+</sup> )	nd	4.25 ± 0.28	0.47 ± 0.04
IC <sub>50</sub> (μM)	> 100	1.27 ± 0.3	0.44 ± 0.16

which occupies both the HP- and ATP-binding sites, has well-defined electron density (Figure 2b).

The overall structure of the protein is similar to that observed in the HPPK·HP·MgAMPCPP complex.<sup>18</sup> The C $\alpha$  trace of the two structures shows some differences only in loop 2, loop 3, and a region near the C terminus. Loop 2 consists of residues 44–50, most of which are involved in HP binding. Loop 3 consists of residues 80–95, most of which are involved in the binding of ATP. A main-chain displacement of ~1.8 Å is observed for residue Asp49 in loop 2 and Lys85 in loop 3. In HPPK·MgHP<sub>4</sub>A, loop 2 moves away from the active center and loop 3 moves further toward the active center when compared with those in the ternary complex. Accordingly, some side chains on the loops have rather differ-

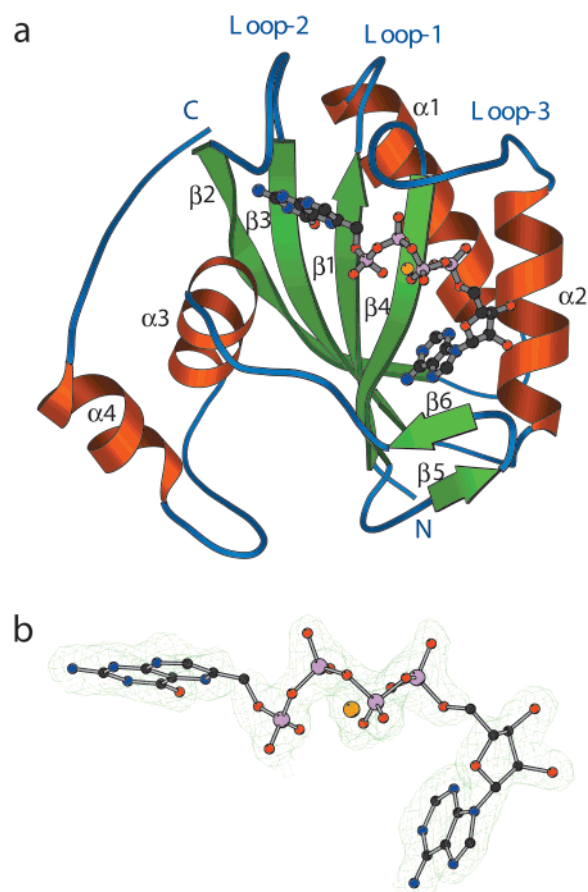


**Figure 2.** (a) Overall structure of the HPPK·MgHP<sub>4</sub>A complex. Secondary structure elements and three flexible loops are labeled according to their order of appearance in the polypeptide chain. (b) Final  $2F_o - F_c$  electron density of the inhibitor and  $Mg^{2+}$  ion contoured at the level of  $1.3\sigma$ . The figure was generated with BOBSCRIPT.<sup>40</sup>

**Table 2.** Strongest Intermolecular Interactions of the C-Terminal Region in the Crystal Lattice of HPPK·MgHP<sub>4</sub>A (this work) and the Ternary Complex HPPK·HP·MgAMPCPP<sup>18</sup>

HPPK·MgHP <sub>4</sub> A	(Å)	HPPK·HP·MgAMPCPP	(Å)
Glu141 OE1–Arg75 NH2	2.90	Asp153 OD1–Arg75 NH2	2.93
Glu141 OE2–Arg75 NH1	2.86	Asp153 OD2–Arg75 NH1	2.87
Asp153 OD1–Arg110 NH1	2.50	His148 ND1–Glu30 OE1	2.58
Asp153 OD2–Glu67 OE1	2.52	Gln145 NE2–Gln80 O	2.91
Arg150 NH2–Asn71 O	2.75		

ent conformations. The largest main-chain atom displacement is observed for Arg150 that is located in the region between  $\alpha$ 4-helix and the C-terminal loop (Figure 2a). The conformational differences are most likely due to the different intermolecular interactions in the two crystals (Table 2). Five hydrogen bonds and 11 van der Waals contacts ( $\leq 3.50$  Å) are found between this region and symmetry-related molecules in HPPK·MgHP<sub>4</sub>A (this work), whereas 4 hydrogen bonds and 7 short contacts are found for HPPK·HP·MgAMPCPP.<sup>18</sup> None of the intermolecular hydrogen bonds in this region is the same between the two structures.

The pterin and adenosine moieties of HP<sub>4</sub>A can be superimposed well with the counterparts in HPPK·HP·MgAMPCPP.<sup>18</sup> The adenosine moiety binds to the protein with the same hydrogen bond pattern in both structures (Figure 3a). The hydrogen bond pattern between the pterin moiety and protein is also the same

except one hydrogen bond between N8 of pterin and HPPK. In HPPK·HP·MgAMPCPP, N8 of HP is hydrogen-bonded to the carbonyl oxygen of Leu45. In HPPK·MgHP<sub>4</sub>A, however, this hydrogen bond does not exist (Figure 3b). Because the pterin moiety of HP<sub>4</sub>A is oxidized, N8 cannot serve as a hydrogen bond donor. Consequently, the carbonyl group of Leu45 flips by  $\sim 180^\circ$  probably due to the unfavorable interaction between the lone pairs of electrons of the nitrogen and oxygen atoms. The C–O bond of the hydroxymethyl group of the pterin moiety rotates by  $\sim 65^\circ$  probably due to the positioning of the phosphate chain.

The  $Mg^{2+}$  coordination is rather different between the two structures. Two  $Mg^{2+}$  ions are found in HPPK·HP·MgAMPCPP,<sup>18</sup> one coordinated with the  $\alpha$ - and  $\beta$ -phosphates and the other with the  $\beta$ - and  $\gamma$ -phosphate groups (Figure 3c). Both  $Mg^{2+}$  ions are coordinated with the carboxyl groups of Asp95 and Asp97. Only one  $Mg^{2+}$  ion is found in HPPK·MgHP<sub>4</sub>A; one oxygen atom from each of the four phosphate groups and two water molecules satisfy the octahedral coordination of the  $Mg^{2+}$  ion (this work, Figure 3d). The two water molecules are hydrogen-bonded to the carboxyl group of Asp97. Asp95 forms salt bridges with both Arg82 and Arg92.

The conformation of the phosphate chain is also different between the two structures, and so their interactions with the protein are different as well (Figure 3c,d). When superimposed, the  $\alpha$ -phosphorus of HP<sub>4</sub>A is close to the counterpart of ATP (0.81 Å), the  $\beta$ - and  $\gamma$ -phosphorus atoms of HP<sub>4</sub>A are close to the  $\beta$ -phosphorus of ATP (2.89 and 2.30 Å, respectively), and the  $\delta$ -phosphorus of HP<sub>4</sub>A is close to the  $\gamma$ -phosphorus of ATP (1.61 Å). In HPPK·MgHP<sub>4</sub>A (this work), Arg82 interacts with the  $\alpha$ -phosphate of HP<sub>4</sub>A and Arg92 forms hydrogen bonds with  $\gamma$ -phosphate (Figure 3d), whereas in HPPK·HP·MgAMPCPP,<sup>18</sup> Arg92 interacts with the  $\alpha$ -phosphate of AMPCPP and Arg82 is not involved in phosphate binding at all (Figure 3c). The side chain of Arg88 in the ternary complex interacts with the oxygen bridge between the  $\beta$ - and  $\gamma$ -phosphates via a water molecule, whereas in HPPK·HP<sub>4</sub>A (this work) it interacts with a  $\beta$ -phosphate oxygen (Figure 3d). Other residues that show differences in substrate/inhibitor binding include Trp89, His115, Tyr116, and Arg121 as shown in Figure 3c,d.

## Discussion

**Bisubstrate Analogue Inhibitor Design.** One of the most effective approaches to enhance the specificity and potency in enzyme inhibition is to design multi-substrate analogue inhibitors.<sup>19,20</sup> This approach has been widely used for designing inhibitors for kinases. A number of potent bisubstrate analogue inhibitors have been made by this approach.<sup>20,21</sup> Classical examples include  $P^1, P^5$ -bis(5'-adenosyl)pentaphosphate (AP<sub>5</sub>A), a potent inhibitor of adenylate kinase,<sup>22</sup> and  $P^1$ -(5-adenosyl)- $P^5$ -(5'-thymidyl)pentaphosphate (AP<sub>5</sub>T), a potent inhibitor of thymidylate kinase.<sup>23</sup> However, not all multisubstrate analogues are strong inhibitors. For example, the bisubstrate analogues of hexokinase  $P^1$ -(5-adenosyl)- $P^3$ -(6-glucosyl)triphosphate and  $P^1$ -(5-adenosyl)- $P^1$ -(6-glucosyl)tetraphosphate are only weak inhibitors of hexokinase with affinities for the enzyme much lower than either substrate ATP or glucose.<sup>24</sup>

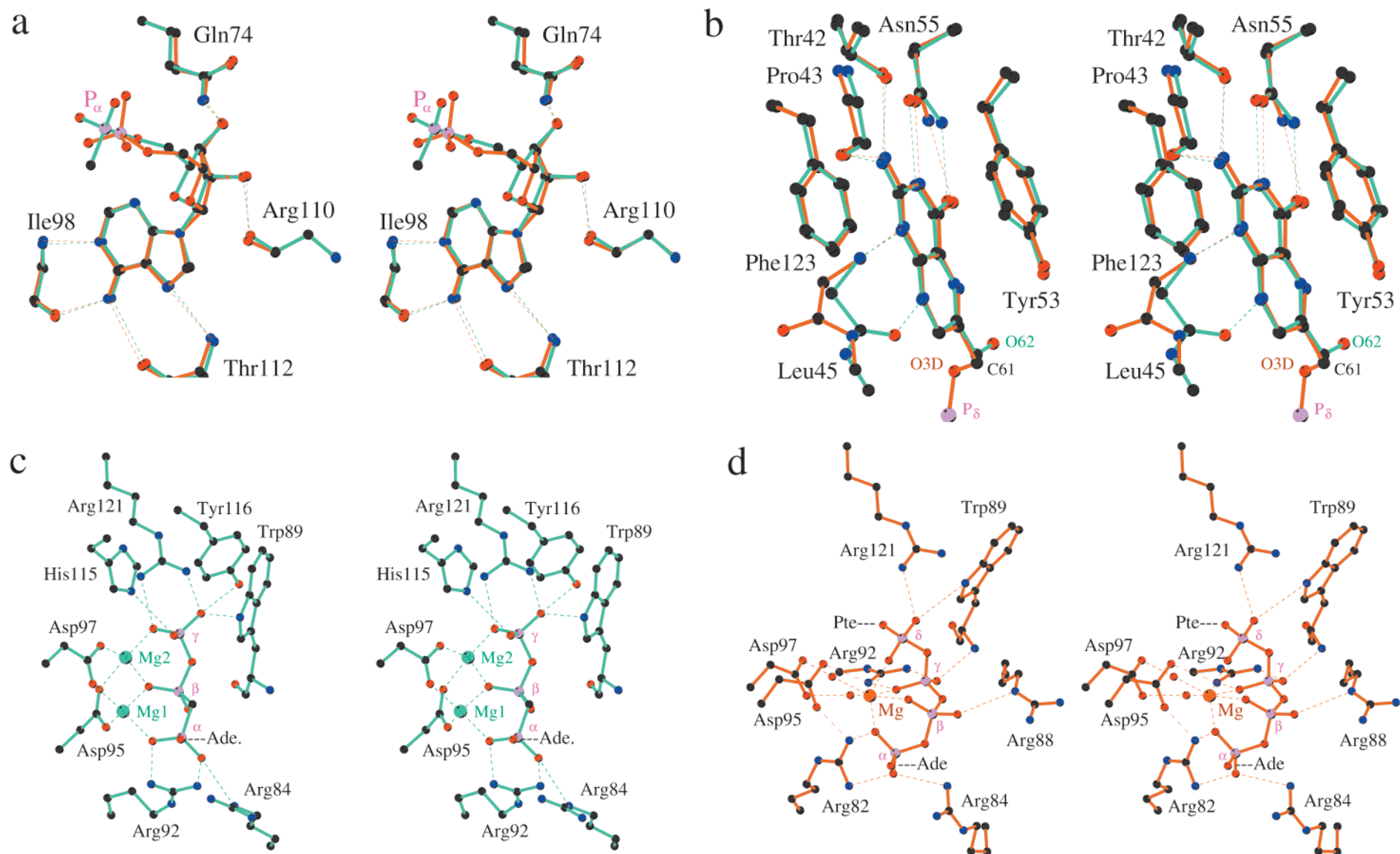


**Figure 3.** Stereoviews of the active-site architecture in HPPK·MgHP<sub>4</sub>A (orange, this work) in alignment with that of HPPK·HP·MgAMPCPP,<sup>18</sup> showing the (a) adenosine-binding site and (b) HP-binding site; (c) binding of the three phosphate groups of AMPCPP in HPPK·HP·MgAMPCPP and (d) binding of the tetraphosphate bridge in HPPK·HP<sub>4</sub>A. Note the presence of 2 Mg<sup>2+</sup> ions in the ternary complex and 1 Mg<sup>2+</sup> ion (orange) in HPPK·MgHP<sub>4</sub>A. The figure was generated with BOBSCRIPT.<sup>40</sup>

The pyrophosphoryl-transfer reaction catalyzed by HPPK is different from the phosphoryl-transfer reactions catalyzed by kinases in that the substitution reaction takes place at  $\beta$ -phosphate. One might expect to lose the interactions between the  $\gamma$ -phosphate of ATP and HPPK when making bisubstrate analogues. Whether the bisubstrate analogue approach works for pyrophosphokinase is not known.

To test whether the bisubstrate analogue approach is effective for making potent inhibitors of HPPK, we have synthesized three bisubstrate analogues (**5**–**7**). Since the pyrophosphoryl-transfer reaction catalyzed by HPPK takes place at  $\beta$ -phosphate, MgADP and 6-hydroxymethylpterin are the appropriate standards for comparing the affinities of the bisubstrate analogues for HPPK. Both compounds are competitive inhibitors of the enzyme. The  $K_d$  values of MgADP<sup>25</sup> and 6-hydroxymethylpterin (Shi et al., unpublished data) are 55 and 36  $\mu$ M, respectively. Since HP<sub>2</sub>A shows little inhibitory activity at 100  $\mu$ M concentration, it must have a much lower affinity for HPPK than MgADP and HP. The  $K_d$  of MgHP<sub>3</sub>A is  $\sim 4$   $\mu$ M, indicating that the affinity of MgHP<sub>3</sub>A for HPPK is  $\sim 12$  and 7 times higher than that of MgADP and 6-hydroxymethylpterin. The affinity of MgHP<sub>4</sub>A for HPPK is  $\sim 116$  and 76 times higher than that of MgADP and 6-hydroxymethylpterin, respectively. The results demonstrate that the bisubstrate analogue approach can produce more potent inhibitors for HPPK.

Why is the affinity of HP<sub>2</sub>A (**5**) for HPPK much lower than that of 6-hydroxymethylpterin or MgADP? Most likely it is due to the fact that the diphosphate link is not long enough to connect pterin and adenosine in their respective binding pockets in the enzyme. As revealed by the crystal structure of HPPK·HP·MgAMPCPP,<sup>18</sup> the distance between the hydroxyl oxygen of the pterin moiety and the 5'-hydroxyl oxygen of the adenosine moiety is 7.2 Å. As shown by the crystal structures of both HPPK·MgHP<sub>4</sub>A (this work) and HPPK·HP·MgAMPCPP,<sup>18</sup> both the pterin and the adenosine moieties are well-fixed in the active center of HPPK by many intermolecular hydrogen bonds. Furthermore, the pterin and adenosine binding pockets are situated on the core of the protein and cannot move toward each other without a major steric clash. Accordingly, the minimum length for the link of a bisubstrate analogue is likely to be  $\sim 7$  Å, and a minimum of three phosphates is needed to connect the pterin and adenosine moieties. With a diphosphate link, probably only one end of **5** (either the pterin moiety or the adenosine moiety) is bound to HPPK leaving the other end dangling in solution.

The next question, then, is why **7** has a much higher affinity for HPPK than **6** if a triphosphate link is long enough to connect the pterin and adenosine moieties. This question is addressed by comparing the crystal structure of HPPK·MgHP<sub>4</sub>A with that of HPPK·HP·MgAMPCPP (Figure 3c,d).<sup>18</sup> As shown in Figure 3c, the  $\gamma$ -phosphate of AMPCPP forms five hydrogen bonds with HPPK. With a triphosphate link, **6** may lose all these electrostatic interactions. With an extra phosphate, **7** is able to keep two of the five electrostatic interactions (Figure 3d).

Although **6** and **7** are potent inhibitors of HPPK, they may have poor bioavailability because of many negative

charges carried by the polyphosphate links. To improve the bioavailability, we will replace the link with neutral ones in designing the next generation of bisubstrate inhibitors. Other improvements may include modification of the pterin moiety of the inhibitors. The crystal structure of HPPK·MgHP<sub>4</sub>A reported here will be very valuable for designing the next generation of bisubstrate inhibitors for HPPK.

**Mechanistic Implications.** It was surprising to find that the side chains of several strictly conserved residues, including those of Gln50, Arg82, and Arg92, point away from the active center when the structure of apo-HPPK was determined,<sup>26</sup> suggesting that significant conformational changes must occur upon binding of the substrates. Indeed, the binding of HP and AMPCPP induces significant conformational changes in the three loops that contain these conserved residues.<sup>18</sup> Similar induced conformational changes occur when **7** binds to HPPK. Loop 2 moves toward the active center by as much as 6.8 Å and loop 3 by as much as 9.2 Å. Loops 2 and 3 are involved in binding of HP and ATP, respectively. All the arginine residues (Arg82, Arg84, Arg88, and Arg92) on loop 3 move toward the active center and interact with the tetraphosphate. The guanidinium groups of Arg82, Arg84, Arg88, and Arg92 move by as much as 15.0, 15.4, 17.3, and 10.9 Å, respectively. The side-chain amide of Gln50 on loop 2 moves toward the active center by 6.6 Å. As a result, it forms a hydrogen bond with the side-chain amide of Asn10 on loop 1 and the carbonyls of Trp89 on loop 3 and Pro47 on loop 2. It is apparent that these parts of the active center are assembled only after the binding of the substrates.

The secondary structure and folding of the N-terminal two-thirds polypeptide chain of HPPK is similar to that of the corresponding part of NDP kinase.<sup>18,27</sup> When the structures of the two enzymes are superimposed, the phosphate-binding regions overlap but the nucleoside-binding regions are in opposite directions. The structural similarity raises the important question whether the two enzymes follow a similar kinetic mechanism. NDP kinase is unique among kinases because it has only one substrate-binding site per subunit and follows a ping-pong mechanism with a phosphohistidine covalent intermediate.<sup>28</sup> However, HPPK has two substrate-binding sites and forms a ternary complex with both substrates.<sup>27</sup> The crystal structure of HPPK·MgHP<sub>4</sub>A clearly shows that the bisubstrate analogue occupies both substrate-binding sites. Furthermore, the substitution of the conserved histidine residue His115 in *E. coli* HPPK causes a slight increase in  $k_{cat}$  rather than abolishing the catalytic activity (Gong et al., unpublished data), ruling out the possibility of the formation of a covalent intermediate involving His115. The results suggest that the HPPK-catalyzed reaction follows a sequential mechanism involving the formation of a ternary complex with both substrates bound.

## Experimental Section

**Materials.** Folic acid, 1,1'-carbonyldiimidazole, and all nucleotides were purchased from Sigma. Sodium borohydride (98%), pyrophosphoric acid (tech.), *n*-tributylamine (99%), sodium perchlorate hydrate (99%), phosphoric acid (99%) and other general organic reagents were purchased from Aldrich. 48% HBr was purchased from Spectrum. Bromine was purchased from Baker. DEAE-cellulose was purchased from

Whatman. TLC sheets silica gel 60 F254 were purchased from Riedel-de Haen. TLC sheets PEI-cellulose F were purchased from EM Science.

**Synthesis of 6-Hydroxymethylpterin (3).** 6-Hydroxymethylpterin was synthesized according to the method of Thijssen.<sup>29</sup> Briefly, 6-formylpterin was obtained by heating a solution of folic acid in 40% hydrogen bromide containing excess bromine at 100 °C for 2 h followed by washing with water and extraction with hot acetone. 6-Hydroxymethylpterin was obtained by reduction of 6-formylpterin with sodium borohydride. The UV and NMR spectra of the 6-hydroxymethylpterin were identical to those of the same compound purchased from Sigma. For kinetic assays, the compound was reduced to 6-hydroxymethyl-7,8-dihydropterin by sodium dithionite as previously described.<sup>30</sup>

**Synthesis of 6-Hydroxymethylpterin Monophosphate (4).** The method for the synthesis of 6-hydroxymethylpterin pyrophosphate<sup>15</sup> was adapted for the synthesis of 6-hydroxymethylpterin monophosphate. Briefly, phosphoric acid was first dried under vacuum for 2 days and then melted and mixed slowly with 6-hydroxymethylpterin at 60–65 °C in a glass-stoppered flask wrapped with aluminum foil. The mixture was stirred and heated at 60–65 °C for 4 h. The product was adsorbed to active charcoal, extracted with 3 N ammonium hydroxide and purified by chromatography on DEAE-cellulose. <sup>1</sup>H NMR: δ 4.94 (d, <sup>3</sup>J = 7.3 Hz, 2H), 8.74 (s, 1H). <sup>31</sup>P NMR: δ 2.84 (s, 1P). FAB-MS (NBA): *m/z* = 272.04; 272.03 for C<sub>7</sub>H<sub>8</sub>N<sub>5</sub>O<sub>5</sub>P, [M - H]<sup>-</sup>.

**Synthesis of Bisubstrate Analogues 5–7.** The bisubstrate analogues were synthesized by coupling adenosine nucleotides to 6-hydroxymethylpterin monophosphate previously synthesized and activated with 1,1'-carbonyldiimidazole.<sup>14,16</sup> Pyridinium form of Dowex 50W-X8 was obtained by allowing the resin to stand with 50% aqueous pyridine. Tributylammonium salts (1 mmol) of AMP, ADP, ATP, and 6-hydroxymethylpterin monophosphate were prepared by first converting their sodium salts to pyridinium salts by chromatography on a Dowex 50W-X8 column. The column was eluted with 50% aqueous methanol. The eluent was evaporated under reduced pressure to 5–10 mL, and then 1 mol equiv of tributylamine/mol of phosphorus and 10–15 mL methanol were added. After 30 min of stirring, the solution was concentrated under vacuum. The residue was dried by repeated addition and evaporation of anhydrous pyridine followed by two 10-mL portions of *N,N*-dimethylformamide (DMF).

To synthesize the bisubstrate analogues, the anhydrous tributylammonium salt of 6-hydroxymethylpterin monophosphate (0.1 mmol) and 1,1'-carbonyldiimidazole (0.5 mmol) both dissolved in 1 mL dry DMF were mixed. After 2 h of stirring at room temperature, 0.7 mmol methanol was added and 30 min later, the anhydrous tributylammonium salt of one of the adenosine nucleotides (0.25 mmol) in a minimal volume of dry DMF was added. After additional 24 h of stirring, the reaction mixture was evaporated to dryness, dissolved in a minimal volume of water and loaded on to a DEAE-cellulose column. The column was eluted with a linear gradient (0–0.8 M) of triethylammonium bicarbonate, pH 7.5. Appropriate fractions were evaporated under vacuum; ethanol was added and evaporated again to remove triethylammonium bicarbonate. The residue was dissolved in a minimal volume of methanol, and 7 mmol sodium perchlorate in 50 mL acetone was added. The precipitated sodium salt was collected by centrifugation and washed with acetone.

The results of NMR and MS analyses of the bisubstrate analogues are summarized as follows. For HP<sub>2</sub>A, <sup>1</sup>H NMR: 4.15–4.53 (m, 5H), 4.95 (d, <sup>3</sup>J = 4.4 Hz, 2H), 5.95 (d, <sup>3</sup>J = 5.13 Hz, 1H), 8.04 (s, 1H), 8.12 (s, 1H), 8.39 (s, 1H). <sup>31</sup>P NMR: -11.04, (broad, 2P). MALDI-MS (ATT): *m/z* = 601.589; 601.08 for C<sub>17</sub>H<sub>20</sub>N<sub>10</sub>O<sub>11</sub>P<sub>2</sub>, [M - H]<sup>-</sup>. For HP<sub>3</sub>A, <sup>1</sup>H NMR: 4.20–4.52 (m, 5H), 4.94 (d, <sup>3</sup>J = 6.6 Hz, 2H), 5.95 (d, <sup>3</sup>J = 4.4 Hz, 1H), 8.00 (s, 1H), 8.17 (s, 1H), 8.41 (s, 1H). <sup>31</sup>P NMR: -10.8, (broad, 1P), -10.94 (broad, 1P), -22.33 (broad, 1P). MALDI-MS (ATT): *m/z* = 680.275; 681.05 for C<sub>17</sub>H<sub>21</sub>N<sub>10</sub>O<sub>14</sub>P<sub>3</sub>, [M - H]<sup>-</sup>.

For HP<sub>4</sub>A, <sup>1</sup>H NMR: 4.30–4.53 (m, 3H), 4.22 (m, 2H), 5.04 (d, <sup>3</sup>J = 7.33 Hz, 2H), 5.88 (d, <sup>3</sup>J = 5.13 Hz, 1H), 8.04 (s, 1H), 8.19 (s, 1H), 8.61 (s, 1H). <sup>31</sup>P NMR: -11.02 (broad, 2P), -22.48 (broad, 2P). MALDI-MS (ATT): *m/z* = 760.729; 761.01 for C<sub>17</sub>H<sub>22</sub>N<sub>10</sub>O<sub>17</sub>P<sub>4</sub>, [M - H]<sup>-</sup>.

**NMR and MS Analyses.** All NMR spectra were recorded at 25 °C on a Varian INOVA 300 spectrometer. The samples were dissolved in D<sub>2</sub>O. <sup>1</sup>H chemical shifts were referenced to the residual water resonance (δ = 4.63 ppm). <sup>31</sup>P chemical shifts were referenced to external 85% phosphoric acid. FAB-MS spectra were recorded on a JEOL JMS-HX 110 spectrometer and 3-nitrobenzyl alcohol (NBA) was used as matrix. MALDI-MS spectra were recorded in the negative mode on a Perspective Biosystem Voyager DE spectrometer and 6-aza-2-thiothymine (ATT) was used as matrix.

**Enzyme Assay.** *E. coli* HPPK was purified as previously described.<sup>31</sup> The inhibition assay was performed in a microtube containing the following components in 100 mM Tris-HCl, pH 8.3: 0.1 mM 6-hydroxymethyl-7,8-dihydropterin, 1.5 mM ATP, 8 mM MgCl<sub>2</sub>, 5 mM DTT, 4.4 nM HPPK, a trace amount of [α-<sup>32</sup>P]ATP, and various amounts of an inhibitor (Hp<sub>2</sub>A, Hp<sub>3</sub>A, or Hp<sub>4</sub>A). The total volume was 200 μL. The reaction was initiated by the addition of ATP at 30 °C. After 30 min, 50 μL of the reaction mixture was transferred to a new microtube containing 50 μL 120 mM EDTA and mixed on a vortex. An aliquot of the reaction mixture was then spotted onto a PEI-cellulose plate. The plate was developed with 0.3 M KH<sub>2</sub>PO<sub>4</sub>. The radioactivity of the plate was measured by a Phosphor-Imager system (Molecular Dynamics Storm 820). IC<sub>50</sub> was obtained by fitting the data to a logistic equation by nonlinear least-squares regression<sup>32</sup> using the software Origin from Microcal.

**Fluorometric Titration.** Protein and ligand stock solutions were made in 100 mM Tris-HCl, pH 8.3, and their concentrations were determined spectrophotometrically using the following extinction coefficients: 21 600 M<sup>-1</sup> cm<sup>-1</sup> at 280 nm for HPPK and 7 000 M<sup>-1</sup> cm<sup>-1</sup> at 366 nm for the bisubstrate inhibitors. A 2-mL diluted inhibitor solution in a fluorometric cuvette was titrated with the protein stock solution. The temperature was regulated at 25 °C by a circulating water bath. Fluorescence was measured on a Spex FluoroMax-2 fluorometer. The excitation wavelength and slit were 364 and 3 nm, respectively, and the emission wavelength and slit were 450 and 5 nm, respectively. A few HPPK preparations showed some fluorescence at the excitation and emission wavelengths. For these HPPK preparations, a control experiment, in which a 2-mL buffer solution was titrated with the protein solution, was performed. The control data was subtracted from the titration data. The corrected titration data was then analyzed by nonlinear least-squares regression using the software Origin and the equation:

$$F_{\text{obs}} = \epsilon_f L_t + \frac{(\epsilon_b - \epsilon_f)(L_t + E_t + K_d - \sqrt{(L_t + E_t + K_d)^2 - 4E_t L_t})}{2}$$

where  $F_{\text{obs}}$  is the observed fluorescence,  $\epsilon_f$  and  $\epsilon_b$  are the fluorescence coefficients of the ligand in the free and protein-bound states, respectively,  $L_t$  is the total concentration of the ligand, and  $E_t$  is the total concentration of HPPK.  $L_t$  and  $E_t$  were varied during the titration process according to the following expressions:

$$L_t = \frac{L_0 V_0}{V_0 + \Delta V}$$

$$E_t = \frac{E_0 \Delta V}{V_0 + \Delta V}$$

where  $E_0$  is the concentration of the HPPK stock solution,  $L_0$  is the initial concentration of the ligand,  $V_0$  is the initial

**Table 3.** Summary of Crystallographic Data Collection, Structure Solution, and Refinement for HPPK·MgHP<sub>4</sub>A

crystal shape	block
crystal dimensions (mm)	0.1 × 0.1 × 0.2
overall (last shell) <sup>a</sup> completeness (%)	89.5 (77.6)
overall (last shell) $R_{\text{sym}}^b$	0.154 (0.338)
overall (last shell) $I/\sigma(I)$	5.9 (2.1)
no. reflns used for refinement: $I2\sigma(I)/\text{all}$	9368/12025
no. reflns used for $R_{\text{free}}$ : $I2\sigma(I)/\text{all}$	480/614
no. least-squares parameters	5668
no. residues/(non-H) atoms	158/1267
no. heterogen atoms	50
no. water oxygen atoms	167
$R_{\text{free}}$ : $I2\sigma(I)/\text{all}$	0.217/0.242
$R$ factor: $I2\sigma(I)/\text{all}$	0.185/0.212
rms deviations from ideal (Å): bond lengths	0.006
rms deviations from ideal (Å): angle distances	0.021
estimated coordinate error (Å)	0.18
Ramachandran statistics: residues in most favored regions (%)	91.2
Ramachandran statistics: residues in additional allowed regions (%)	8.8

<sup>a</sup> Resolution range 1.92–1.85 Å. <sup>b</sup>  $R_{\text{sym}} = \sum |I - \langle I \rangle| / \sum I$ . Friedel pairs were merged.

volume of the titration, and  $\Delta V$  is the total volume of the added HPPK solution.

**Crystallization of HPPK·MgHP<sub>4</sub>A.** The crystals were grown at room temperature (293 K) in hanging drops. The protein stock solution contained 10 mg/mL HPPK, 35 mM HP<sub>4</sub>A, 50 mM MgCl<sub>2</sub> and 10 M Tris-HCl (pH 8.0); the reservoir solution consisted of 28% (w/v) PEG 4000, 0.18 M ammonium acetate, 0.15 M sodium acetate (pH 5.5), and 10% (v/v) glycerol. The drops were composed with equal volumes of protein and reservoir solutions. The crystals appeared within 3 days, and after 1 week they were ready for X-ray data collection (Table 3).

**Data Collection, Structure Solution, and Refinement.** The diffraction data were collected from a single crystal at a cryogenic temperature (100 K; Oxford cryosystem), using a Rigaku rotating anode operated at 50 kV and 100 mA with a MAR345 image plate system. The crystal diffracted to 1.85 Å resolution. Data processing was carried out with the HKL2000 program suite.<sup>33</sup> The data set consisted of 12 732 unique reflections from a total of 39 784 measurements and was 89.5% complete. The internal  $R$  factor between symmetry-related reflections was 0.15 (Table 3). The complex crystallized in the orthorhombic space group  $P2_12_12_1$  with 1 HPPK·HP<sub>4</sub>A complex and 1 Mg<sup>2+</sup> ion in the asymmetric unit. The unit-cell dimensions were  $a = 38.053$  Å,  $b = 61.857$  Å,  $c = 67.106$  Å, and  $\alpha = \beta = \gamma = 90^\circ$ . The solvent content of the crystals was 39.8%, and the Matthews coefficient ( $V_m$ )<sup>34</sup> was 2.1. The crystal structure was solved by molecular replacement with the program suite AmoRe.<sup>35</sup> The search model was the crystal structure of apo-HPPK<sup>26</sup> without solvent molecules. The solution from molecular replacement after rotational and translational search consisted of one molecule and had a correlation coefficient of 0.59 and a crystallographic  $R$  factor of 0.38. Structure refinement involved 4 rounds of the simulated annealing procedure of CNS<sup>36</sup> and 14 rounds of least-squares refinement using SHELXL-97<sup>37</sup> for X-ray data in the resolution range 40.0–1.85 Å. Model building during the initial stage of refinement involved the adjustment of loop conformation and side chains according to electron density. Further model building was focused on the positioning of the HP<sub>4</sub>A molecule according to difference electron density above  $3\sigma$ , and the addition of solvent molecules was done at a later stage. All model building and adjustments were done using the O graphics package.<sup>38</sup> The final model of the structure consisted of all nonhydrogen atoms of the polypeptide chain (158 residues), 1 HP<sub>4</sub>A molecule, 1 Mg<sup>2+</sup> ion, 1 Cl<sup>-</sup> ion, and 167 water molecules. All protein atoms, inhibitor, ions and solvent molecules had evident electron densities above  $1\sigma$  on the  $2F_o - F_c$  map, except for the side chains of Arg84, Lys85, and Glu87, which are located at the surface of the molecule. The

final  $R$  factor and  $R_{\text{free}}$  were 0.185 and 0.217, respectively, for all data with their intensities equal to or above  $2\sigma$  (Table 3). The final electron density did not show more interpretable features. The root-mean-square (rms) deviations for bond lengths and angle distances were 0.006 and 0.021 Å, respectively (Table 3). The structure has been assessed using PROCHECK,<sup>39</sup> showing that 91.2% of the residues are in the most favored regions of the Ramachandran plot and no residue falls into disallowed or generously allowed regions (see Table 3).

**Acknowledgment.** We thank Dr. Nicholas V. Cozzi for advice on IC<sub>50</sub> measurements. This work was supported in part by NIH Grant GM51901 awarded to H.Y.

**Supporting Information Available:** Stereodiagrams showing the structural alignments between HPPK·MgHP<sub>4</sub>A (this work) and HPPK·HP·MgAMPCPP<sup>18</sup> and between HPPK·MgHP<sub>4</sub>A (this work) and apo-HPPK.<sup>26</sup> This material is available free of charge via the Internet at <http://pubs.acs.org>.

## References

- (1) Cohen, M. L. Epidemiology of drug resistance: implications for a post-antimicrobial era. *Science* **1992**, *257*, 1050–1055.
- (2) Neu, H. C. The crisis in antibiotic resistance. *Science* **1992**, *257*, 1064–1072.
- (3) Kunin, C. M. Resistance to antimicrobial drugs – a worldwide calamity. *Ann. Intern. Med.* **1993**, *118*, 557–561.
- (4) Levy, S. B. Antimicrobial resistance: A global perspective. *Adv. Exp. Med. Biol.* **1995**, *390*, 1–15.
- (5) Murray, B. E. Antibiotic resistance. *Adv. Intern. Med.* **1997**, *42*, 339–367.
- (6) *World Health Organization Report on Infectious Diseases: Removing Obstacles to Healthy Development*; World Health Organization: Geneva, 1999.
- (7) Shiota, T. Biosynthesis of folate from pterin precursors. *Chemistry and Biochemistry of Foliates*; John Wiley & Sons: New York, 1984; pp 121–134.
- (8) Blakley, R. L.; Benkovic, S. J. Chemistry and Biochemistry of Foliates. *Foliates and Pterins*; John Wiley & Sons: New York, 1984.
- (9) Hughes, D. T. D. Sulphonamides. *Antibiotic and Chemotherapy*, 7 ed.; Churchill Livingstone: New York, 1997; pp 460–468.
- (10) Hughes, D. T. D. Diaminopyrimidines. *Antibiotic and Chemotherapy*, 7 ed.; Churchill Livingstone: New York, 1997; pp 346–356.
- (11) Talarico, T. L.; Dev, I. K.; Dallas, W. S.; Ferone, R.; Ray, P. H. Purification and partial characterization of 7,8-dihydro-6-hydroxymethylpterin-pyrophosphokinase and 7,8-dihydropteroyl synthase from *Escherichia coli* MC4100. *J. Bacteriol.* **1991**, *173*, 7029–7032.
- (12) Talarico, T. L.; Ray, P. H.; Dev, I. K.; Merrill, B. M.; Dallas, W. S. Cloning, sequence analysis, and overexpression of *Escherichia coli* folK, the gene coding for 7,8-dihydro-6-hydroxymethylpterin-pyrophosphokinase. *J. Bacteriol.* **1992**, *174*, 5971–5977.
- (13) Switzer, R. L. Phosphoribosylpyrophosphate synthetase and related pyrophosphokinases. *The Enzymes*, 3rd ed.; Academic Press: New York, 1974; pp 607–629.
- (14) Hoard, D. E.; Ott, D. G. Conversion of mono- and oligodeoxyribonucleotides to 5'-triphosphates. *J. Am. Chem. Soc.* **1965**, *87*, 1785–1788.
- (15) Ho, R. I.; Corman, L.; Foye, W. O. Synthesis and biological evaluation of 2-amino-4-hydroxy-6-hydroxymethylpteridine pyrophosphate. *J. Pharm. Sci.* **1974**, *1472*–1476.
- (16) Bone, R.; Cheng, Y. C.; Wolfenden, R. Inhibition of thymidine kinase by P<sup>1</sup>-(adenosine-5')-P<sup>5</sup>-(thymidine-5')-pentaphosphate. *J. Biol. Chem.* **1986**, *261*, 5731–5735.
- (17) Davies, L. C.; Stock, J. A.; Barrie, S. E.; Orr, R. M.; Harrap, K. R. Dinucleotide analogues as inhibitors of thymidine kinase, thymidylate kinase, and ribonucleotide reductase. *J. Med. Chem.* **1988**, *31*, 1305–1308.
- (18) Blaszczyk, J.; Shi, G.; Yan, H.; Ji, X. Catalytic center assembly of 6-hydroxymethyl-7,8-dihydropterin pyrophosphokinase as revealed by the crystal structure of a ternary complex at 1.25 Å resolution. *Structure* **2000**, *8*, 1049–1058.
- (19) Broom, A. D. Rational Design of Enzyme–Inhibitors – Multi-substrate Analogue Inhibitors. *J. Med. Chem.* **1989**, *32*, 2–7.
- (20) Radzicka, A.; Wolfenden, R. Transition state and multisubstrate analogue inhibitors. *Methods Enzymol.* **1995**, *249*, 284–312.
- (21) Liu, M.; Haddad, J.; Azucena, E.; Kotra, L. P.; Kirzhner et al. Tethered bisubstrate derivatives as probes for mechanism and as inhibitors of aminoglycoside 3'-phosphotransferase. *J. Org. Chem.* **2000**, *65*, 7422–7431.

- (22) Lienhard, G. E.; Secemski, I. I. P<sup>1</sup>,P<sup>5</sup>-di(adenosine-5')pentaphosphate, a potent multisubstrate inhibitor of adenylate kinase. *J. Biol. Chem.* **1973**, *248*, 1121–1123.
- (23) Bone, R.; Cheng, Y. C.; Wolfenden, R. Inhibition of adenosine and thymidylate kinases by bisubstrate analogues. *J. Biol. Chem.* **1986**, *261*, 16410–16413.
- (24) Danenberg, P. V.; Danenberg, K. D. Inhibition of hexokinase by multisubstrate analogues. *Biochim. Biophys. Acta* **1977**, *480*, 351–356.
- (25) Shi, G.; Gong, Y.; Savchenko, A.; Zeikus, J. G.; Xiao, B. et al. Dissecting the nucleotide binding properties of *Escherichia coli* 6-hydroxymethyl-7,8-dihydropterin pyrophosphokinase with fluorescent 3'(2')-o-anthraniloyladenine 5'-triphosphate. *Biochim. Biophys. Acta* **2000**, *1478*, 289–299.
- (26) Xiao, B.; Shi, G.; Chen, X.; Yan, H.; Ji, X. Crystal Structure of 6-Hydroxymethyl-7,8-dihydropterin Pyrophosphokinase, a Potential Target for Development of Novel Antimicrobial Agents. *Structure* **1999**, *7*, 489–496.
- (27) Stammers, D. K.; Achari, A.; Somers, D. O.; Bryant, P. K.; Rosemond, J. et al. 2.0 Å X-ray structure of the ternary complex of 7,8-dihydro-6-hydroxymethylpterinpyrophosphokinase from *Escherichia coli* with ATP and a substrate analogue. *FEBS Lett.* **1999**, *456*, 49–53.
- (28) Hengge, A. C. Transfer of the PO<sub>3</sub><sup>2-</sup> group. *Comprehensive Biological Catalysis*; Academic Press: San Diego, 1998; pp 517–542.
- (29) Thijssen, H. H. W. A simple method for preparing 2-amino-4-hydroxy-6-formylpteridine, a precursor of the pteridine substrate of dihydropteroate biosynthesis. *Anal. Biochem.* **1973**, *54*, 609–611.
- (30) Scrimgeour, K. G. Methods for reduction, stabilization, and analyses of folates. *Methods Enzymol.* **1980**, *66*, 517–523.
- (31) Shi, G.; Gao, J.; Yan, H. <sup>1</sup>H, <sup>13</sup>C and <sup>15</sup>N resonance assignments of *Escherichia coli* 6-hydroxymethyl-7,8-dihydropterin pyrophosphokinase and its complex with MgAMPPCP. *J. Biomol. NMR* **1999**, *14*, 189–190.
- (32) Graeser, D.; Neubig, R. R. Methods for the study of receptor/G-protein. *Signal Transduction*; IRL Press: Oxford, 1992; pp 1–30.
- (33) Otwinowski, Z.; Minor, W. Processing of X-ray diffraction data collected in oscillation mode. *Methods Enzymol.* **1997**, *276*, 307–326.
- (34) Matthews, B. W. Solvent content of protein crystals. *J. Mol. Biol.* **1968**, *33*, 491–497.
- (35) Navaza, J. An automated package for molecular replacement. *Acta Crystallogr.* **1994**, *A50*, 157–163.
- (36) Brünger, A. T.; Adams, P. D.; Clore, G. M.; DeLano, W. L.; Gros, P. et al. Crystallography and NMR system (CNS): A new software system for macromolecular structure determination. *Acta Crystallogr.* **1998**, *D54*, 905–921.
- (37) Sheldrick, G. M.; Schneider, T. R. SHELXL: high-resolution refinement. *Methods Enzymol.* **1997**, *277*, 319–343.
- (38) Jones, T. A.; Zou, J. Y.; Cowan, S. W.; Kjeldgaard, M. Improved methods for building protein models in electron density maps and the location of errors in these models. *Acta Crystallogr.* **1991**, *A47*, 110–119.
- (39) Laskowski, R. A.; MacArthur, M. W.; Moss, D. S.; Thornton, J. M. PROCHECK: a program to check the stereochemical quality of protein structures. *J. Appl. Crystallogr.* **1993**, *26*, 283–291.
- (40) Esnouf, R. M. An extensively modified version of MolScript that includes greatly enhanced coloring capabilities. *J. Mol. Graph Model.* **1997**, *15*, 132–134.

JM0004493